*remote sensing*

MDPI

*Article*

# Predicting Dust-Storm Transport Pathways Using a Convolutional Neural Network and Geographic Context for Impact Adaptation and Mitigation in Urban Areas

**Mahdis Yarmohamadi [1], Ali Asghar Alesheikh [1], Mohammad Sharif [2] and Hossein Vahidi [3,*]**

[1] Department of Geospatial Information Systems, K. N. Toosi University of Technology, Tehran 15433-19967, Iran; myarmohamadi@email.kntu.ac.ir (M.Y.)
[2] Department of Geography, University of Hormozgan, Bandar Abbas 3995, Iran
[3] Department of Geography, Ferdowsi University of Mashhad, Mashhad 91779-48974, Iran
* Correspondence: hossein.vahidi@um.ac.ir

**Abstract:** Dust storms are natural disasters that have a serious impact on various aspects of human life and physical infrastructure, particularly in urban areas causing health risks, reducing visibility, impairing the transportation sector, and interfering with communication systems. The ability to predict the movement patterns of dust storms is crucial for effective disaster prevention and management. By understanding how these phenomena travel, it is possible to identify the areas that are most at risk and take appropriate measures to mitigate their impact on urban environments. Deep learning methods have been demonstrated to be efficient tools for predicting moving processes while considering multiple geographic information sources. By developing a convolutional neural network (CNN) method, this study aimed to predict the pathway of dust storms that occur in arid regions in central and southern Asia. A total of 54 dust-storm events were extracted from the modern-era retrospective analysis for research and applications, version 2 (MERRA-2) product to train the CNN model and evaluate the prediction results. In addition to dust-storm data (aerosol optical depth (AOD) data), geographic context information including relative humidity, surface air temperature, surface wind direction, surface skin temperature, and surface wind speed was considered. These features were chosen using the random forest feature importance method and had feature importance values of 0.2, 0.1, 0.06, 0.03, and 0.02, respectively. The results show that the CNN model can promisingly predict the dust-transport pathway, such that for the 6, 12, 18, and 24-h time steps, the overall accuracy values were 0.9746, 0.975, 0.9751, and 0.9699, respectively; the F1 score values were 0.7497, 0.7525, 0.7476, and 0.6769, respectively; and the values of the kappa coefficient were 0.7369, 0.74, 0.7351, and 0.6625, respectively.

**Keywords:** movement prediction; moving process; deep learning; dust storms; MERRA-2; urban resilience and preparedness



**Citation:** Yarmohamadi, M.; Alesheikh, A.A.; Sharif, M.; Vahidi, H. Predicting Dust-Storm Transport Pathways Using a Convolutional Neural Network and Geographic Context for Impact Adaptation and Mitigation in Urban Areas. *Remote Sens.* **2023**, *15*, 2468. https://doi.org/10.3390/rs15092468

Academic Editors: Giorgos Mallinis and Ifigeneia Theodoridou

Received: 19 March 2023
Revised: 30 April 2023
Accepted: 5 May 2023
Published: 8 May 2023



## 1. Introduction

Fueled by climate change, dust storms have increased considerably in recent years, impacting communities thousands of kilometers away from their origin [1]. According to the World Meteorological Organization, a dust storm is defined as "strong winds that lift large amounts of sand and dust from bare, dry soils into the atmosphere, transporting them hundreds to thousands of kilometers away" [2]. Dust storms, which commonly originate in arid and semi-arid areas (e.g., China, Central Asia, the Arabian Peninsula, and Northern Africa), significantly impact Earth's systems and are regarded as a significant environmental threat [3]. This dynamic phenomenon includes four stages: land degradation, wind erosion, transport (movement), and deposition [4]. Dust storms occur when the wind erosion exceeds the ability of the soil to resist surface erosion. This erosion is caused by the movement of soil particles by the wind. The wind lifts the degraded soil particles from

the ground and moves them thousands of kilometers away. Each year, approximately 2000 million tons of dust are transmitted into the atmosphere, of which 1500 million tons are deposited on land and 500 million tons into the ocean [5].

Dust storms have a wide range of impacts on urban and rural areas [6]. Previous studies have indicated that the impacts of dust storms in urban areas are significantly higher in cities than in rural regions due to the large populations, level of infrastructure, and economic activities [7,8]. In urban areas, dust storms have numerous adverse effects on the daily lives of citizens and infrastructure, such as reducing visibility, impairing the transportation sector, causing road accidents, and interfering with communication systems [9]. Various studies have investigated the short- and long-term effects of dust storms on the health of city dwellers. According to health and safety studies, dust particles have adverse effects on human health and cause respiratory and cardiovascular diseases [10]. For example, studies in Seoul City, Korea, have shown that Asian dust events resulted in an increase of 22% in asthma treatment rates [11]. The findings of several studies in the context of Iranian cities also show that the increase in dust storms in recent years has had a significant effect on respiratory mortality and morbidity [12]. In the urban and peri-urban agriculture sectors, except for a few positive impacts of dust storms, they have negatively impacted soil productivity and crop production and, consequently, revenue [13,14]. Therefore, spatiotemporal monitoring, modeling, and forecasting dust-storm phenomena and developing early warning systems can play an important role in mitigating and preventing their environmental, health, and socioeconomic consequences in human settlements, particularly in urban areas.

Remote-sensing technology plays a crucial role in monitoring dust storms at different spatial and temporal resolutions and in predicting their transport pathways. Satellite-based sensors, ground-based lidars, and radar systems can provide high spatial and temporal resolution data for various atmospheric parameters, including aerosol optical depth (AOD), dust concentration, wind speed, and wind direction. Satellite-based remote sensing platforms such as the moderate resolution imaging spectroradiometer (MODIS) are commonly used to estimate AOD. AOD measures the amount of light that is blocked by aerosols from passing from the ground to the atmosphere. AOD can be measured using satellite remote sensing and ground-based observations [15,16]. Zhang et al. [17] used MODIS data to predict the transport pathways of dust storms in East Asia. Kaskaoutis et al. [18] focused on the detection of the dust source region and monitoring of the transport of the dust plume from its primary outflow to final deposition. They used different remote-sensing technologies, including satellite imagery, ground-based lidar, and air-quality monitoring networks, to study dust storms. The authors highlighted the importance of combining remote sensing and modeling approaches to gain a more comprehensive understanding of dust storms in the Mediterranean. Numerical models can be used in conjunction with remote-sensing data to improve the accuracy of dust-storm transport pathway prediction. Li et al. [19] used the HYSPLIT model in combination with MODIS AOD data to predict the transport pathways of a dust storm that occurred in China. They found that the use of remote-sensing data improved the accuracy of their predictions compared to simulations that did not utilize these data.

The modern-era retrospective analysis for research and application (MERRA-2) dataset [20], which is used in this research, is produced by replicating a set of satellite and ground-based AOD data and has a temporal resolution of one hour. This enables the continuous investigation of dust particles, particularly for the identification of transport mechanisms [21]. Given the fine resolution of the MERRA-2 dataset, time-series analyses can be conducted to predict the transport pathways of dust particles. This analysis not only reveals the urban areas vulnerable to dust storms but also characterizes the event's durability over urban areas and the duration of the events. Dust storms are natural phenomena characterized by the movement of dust particles in the atmosphere. Unlike moving point objects (MPOs) such as humans and vehicles, which maintain a constant size [22], the size of dust storms is constantly changing. This makes them capable of impacting large areas in a

short period of time. MPOs are typically investigated by analyzing their trajectories [23,24]. While dust storms have severely affected residents and their physical assets, particularly in cities and metropolitan areas, few researchers have focused on predicting dust-storm pathways thus far, considering dust storms as MPOs. In this regard, NOAA's HYSPLIT model [25] was used to identify dust sources and model their trajectories in different study areas in Australia [26], China [27,28], and Kazakhstan and Uzbekistan [29]. This model is based on meteorological data, and its accuracy depends on the accuracy of the meteorological data [30]. Trajectory analysis is straightforward, and various environmental parameters (e.g., wind speed and wind direction) can be annotated as trajectories. However, dust storms are dynamic processes, so the area they cover (size) and the changes in location (movement) become significant. Robust tools are required to model the dynamic mechanisms of dust storms and investigate the environmental factors that stimulate their movement.

The movement of dust storms is highly influenced by their surrounding environment, which is known as the geographic context [31,32]. Precipitation, temperature, humidity, wind speed, and wind direction are prominent geographical contexts [33]. The variety of contextual information and the large quantity of dust-storm events make their transport pathway prediction challenging. Deep-learning methods have been demonstrated to be fast, accurate, and efficient tools for predicting movement processes while considering multiple geographic contexts. For example in wildfire-spread modeling, the gated recurrent unit (GRU) and long short-term memory (LSTM) [34], convolutional neural network (CNN) [35], and CNN and LSTM [36] models have been developed based on elevation, wind direction, wind speed, temperature, humidity, precipitation, and drought information. In oil-spill modeling, LSTM [37] and CNN [38] models have been developed to study the movement of oil slicks. The remarkable performance of CNNs in the above dynamic processes makes them a promising tool for dust-storm pathway prediction.

The objective of this study was to present a novel approach for predicting dust-storm transport pathways over the next 24 h. By leveraging the hierarchical nature and high-level feature extraction capabilities of the CNN model, along with the diverse geographic-context information embedded in a dust-storm event, our study aimed to (i) develop a CNN-based architecture for accurately predicting dust-storm pathways, (ii) explore the potential of the MERRA-2 hourly AOD dataset to enhance dust-storm prediction, and (iii) investigate the impact of geographic-context information on the accuracy of dust-storm prediction. Our proposed method can effectively identify locations, including urban areas, that are susceptible to dust particles for up to 24 h following a storm's onset, as well as determine the duration of the storm.

## 2. Materials and Methods

### *2.1. Study Area*

An arid area in Central and South Asia that lies at 25°–42.5° N and 56°–73.5° E was chosen as the study area. It covers an approximate area of 2,750,000 km$^2$ and includes parts of Iran, Afghanistan, Pakistan, Tajikistan, Turkmenistan, and Uzbekistan (Figure 1). These countries have faced the most severe dust storms in recent years. Dust storms in this region have dramatically impacted the various dimensions of human lives and the physical landscapes of the region, particularly the daily lives and physical spaces of millions of people who live in the cities and metropolitan zones in the study area. The region is characterized by a complex topography with mountains and large desert plateaus. The dry plains of Hamun and the dry lake beds surrounding the South Aral Sea, and the deserts in eastern Pakistan are the main sources of dust storms that occur in spring and summer. Low precipitation rates, high temperatures, and low pressures have made these areas suitable for dust-storm occurrence. There are two major types of dust storms in this area according to our dataset. One of them originates in Turkmenistan and lasts for one to two days in the region. The other, which is more severe, originates in Pakistan and lasts for more than three days.

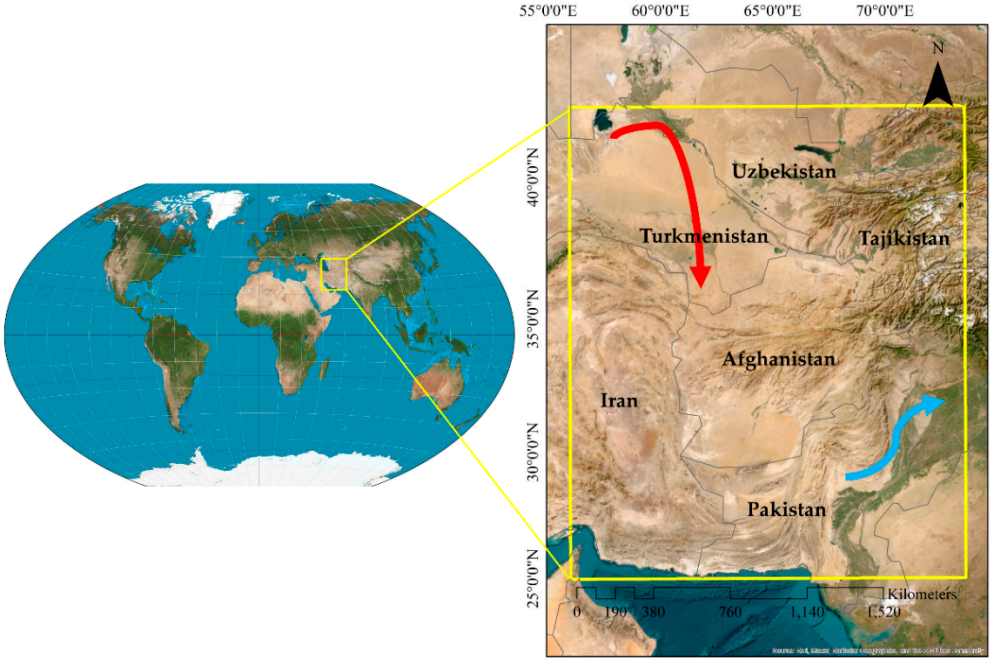


**Figure 1.** The location of the study area and the schematic pathway of a sample dust-storm originate from (1) Turkmenistan (in red) and (2) Pakistan (in blue).

In recent years, Central and South Asia have experienced several severe dust storms that have caused damage and disruption. In April 2022, a severe dust storm hit the city of Mary in Turkmensitan [39], causing power outages and damage to buildings and infrastructure. Dust storms are a recurring problem in Turkmenistan, particularly in the Karakum Desert, which covers several parts of the country. The Central Karakum Desert, characterized by sandy terrain, experiences the highest mean annual frequency of dust storms during spring, which occurs for an average of 67 days. The western region of Turkmenistan reported the maximum number of dust-storm days, with a total of 146 days recorded [40]. In May 2021, a severe dust storm hit Karachi, the largest city in Pakistan, causing several deaths, injuries, and damage to buildings and infrastructure [34]. Dust storms are a recurring problem in Central and South Asia, particularly in arid and semi-arid regions, and their frequency and intensity have been increasing in recent years, which is believed to be linked to climate change and environmental degradation.

### *2.2. Data Sources*

Surface-dust concentrations from 1980 to 2023 are provided by MERRA-2 [20]. MERRA-2 is a satellite-based reanalysis model generated by the Global Modelling and Assimilation Office (GMAO) of NASA [41]. The aerosol model is developed by combining AOD from the advanced very high-resolution radiometer (AVHRR), multi-angle imaging spectroradiometer (MISR), MODIS AOD datasets, and aerosol robotic network (AERONET) ground-based observations [42]. The efficiency of MERRA-2 AOD has been validated in several studies [43,44].

In this research, we use the "dust extinction aerosol optical thickness (AOT) 550 nm" from MERRA-2 to obtain the AOD dataset. The AOD dataset is published hourly with a spatial resolution of $0.5^\circ \times 0.625^\circ$ and is used for hourly prediction of dust-storm pathways. A total of 54 dust-storm events, containing 3820 storm hours between 2000 and 2021, were extracted from the MERRA-2 AOD dataset.

CNNs require input data that are manually annotated with specific tags or labels to describe the content of an image. In machine learning, large amounts of data are often labeled manually for training classifiers and modeling features, which is time-consuming and tedious [45]. To execute this process automatically, we develop an unsupervised and

automatic labeling algorithm that uses the Otsu threshold [46]. Otsu thresholding is a method that automatically determines the optimal threshold value for image segmentation. Once the threshold value has been determined, all pixels with values above it are labeled as class one (dust pixels), and those pixels below are labeled as class zero (not dust pixels). The hourly images of a dust storm were classified into binary classes using the Otsu threshold. The average of these threshold values for every image was used to produce binary-labeled images.

The MERRA-2 provides various types of environmental information. In order to select the most effective parameters among the relevant features (including relative humidity, surface air temperature, surface skin temperature, surface wind speed, surface wind direction, 10-m above-ground wind direction, and 50-m above-ground wind direction) for predicting the dust-storm pathway and reduce the computational cost, a feature selection approach was applied. We used the random forest feature importance (RFFI) technique [47] to measure and order parameters based on their importance. RFFI identifies the most important features or variables in the dataset for predicting a particular outcome. It trains a random forest model on the dataset and then evaluates the importance of each feature based on its contribution to the accuracy of the model. RFFI is a filter feature selector that considers the ensemble's average overall reduction in node impurities as a result of the splitting of a given feature. In order to determine the importance of each feature, the mean decrease impurity (MDI) [48] was used, which measures the decrease in impurity (or increase in purity) in the decision tree when a particular feature is used for splitting. The higher the MDI score, the more important the features. The RFFI calculates the MDI score for each feature across all decision trees in the model, and then averages the scores to obtain a final importance score for each feature [49]. The results show that relative humidity, surface air temperature, surface wind direction (including U and V components of surface wind direction), surface skin temperature, and surface wind speed have the greatest influence on the dust-storm pathway (for more details, see: Section 3).

Data standardization is the process of transforming data before it is fed into an algorithm. Standardization helps to ensure that all features are on the same scale so that the model learns from them equally. Standardization also helps to reduce the effect of outliers, which can have a significant impact on model performance. In this research, the features were standardized using the min–max scaler. It adjusts data from 0 to 1 using the minimum and maximum values of the data [50]. Equation (1) shows the min–max scaler normalization:

$$f = \frac{f - f_{min}}{f_{max} - f_{min}} \quad (1)$$

where $f_{min}$ and $f_{max}$ indicate the minimum and maximum values of the data, respectively.

### *2.3. Methodology*

The framework of our approach consists of three major parts: the model input, prediction model, and model output (Figure 2). The data (3796 storm hours from the total of 3820 storm hours) were divided into 3036 training samples (=80% of the data), 380 test samples (=10% of the data), and 380 validation samples (=10% of the data). The input of the CNN model includes the raw MERRA-2 AOD data (image) at time step $t - 1$ and geographic-context information at time step $t - 1$, and the output includes the predicted dust-storm images over 24 h (t to t + 24). The labeled AOD data layers were also used as the target layers in the training phase of the CNN model.

The transport of dust particles is highly affected by the geographic context; thus, the AOD dataset and the geographic-contextual information (i.e., contextual information) were stacked to construct the input for the CNN layer. We faced a time-series problem, so the raw AOD image and contextual information corresponding to each hour of a storm with dimensions of $140 \times 143$ pixels were given as the input. Thus, the spatiotemporal features of the input data were extracted by the CNN, and the prediction of the proposed model was achieved.

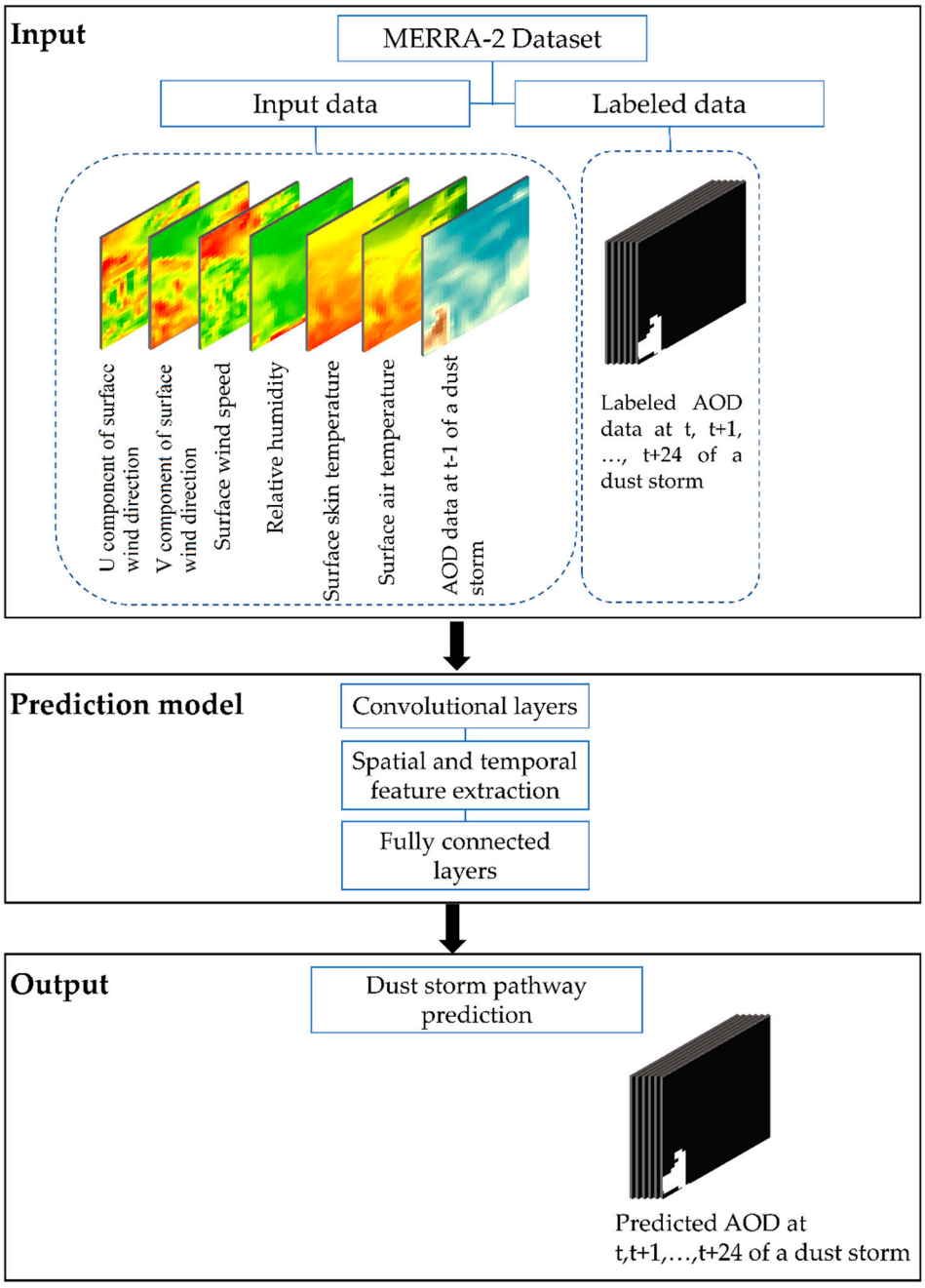


**Figure 2.** Framework for the transport pathway prediction of dust storms.

#### 2.3.1. Convolutional Neural Network

The CNN model, which is a type of artificial neural network, was first introduced by LeCun et al. [51] and developed in [52]. The CNN model performs well in image processing [52] and is suitable for application to time-series analysis [53]. The main advantage of this neural network is that it recognizes important features automatically, without human intervention [54]. CNNs are composed of a set of multilayer interconnected neural networks; therefore, they can hierarchically extract high-, medium-, and low-level features. Early layers extract low-level features, such as edges, and trailing layers extract high-level features, such as the image structure [55]. Feature maps are obtained by multiplying the weight of each kernel by a small part of the input image. Each feature map is used as input to the next layer. Convolutional layers are typically determined based on the convolution kernel size and depth of the output feature map (i.e., the number of filters). Therefore,

the kernel size and number of filters should be chosen such that the extracted features are decisive for the existing problem [56]. The general architecture of a CNN is shown in Figure 3.

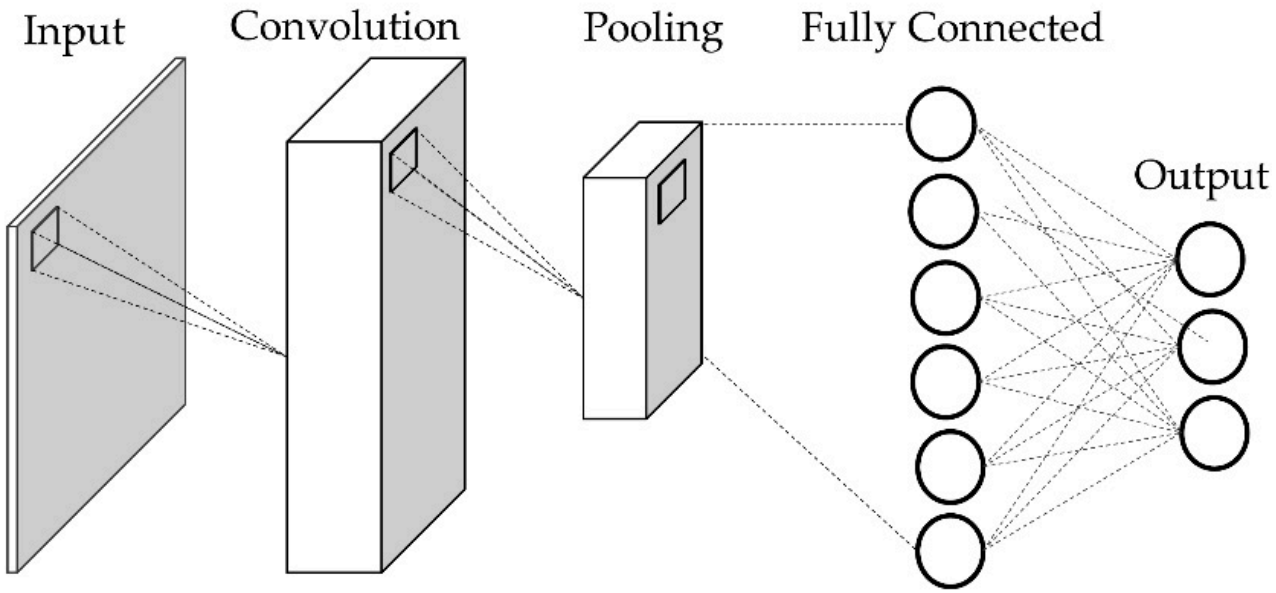


**Figure 3.** Generic CNN architecture.

A CNN consists of convolutional and pooling layers [57]. After each convolutional layer, a pooling layer can be added. As each window can contain common pixels, it is possible to produce several feature maps that are very similar. To reduce the variance of the extracted features, pooling layers are applied after each convolutional layer using simple operations such as maximization or averaging [55]. This layer leads to a reduction in the network parameters, which accelerates the training of the network and makes it possible to handle the overfitting problem [54].

A rectified linear unit (ReLU) [58] is usually applied as an element-wise nonlinear activation function for each component of the feature map. The ReLU function is advantageous because it adds nonlinearity to the network [58]. Compared to conventional gradient descent functions, such as the hyperbolic tangent or sigmoid, ReLU significantly accelerates the training phase [35].

#### 2.3.2. Proposed CNN Architecture

Our developed model contains 15 different layers, including 12 CNN layers, 2 fully connected layers, and a flattened layer (Figure 4). These layers are placed in four main blocks: feature extraction, multiscale feature extraction, filtering multiscale features, and the prediction block. The first block contains two convolutional layers with 64 and 128 $3 \times 3$ filters. Multiscale features were obtained by passing the output of the first block through four convolutional layers with dilation rates of 3, 6, 12, and 1, including 32 filters of size $3 \times 3$ in each layer. In the third block, a convolutional layer with 32 $1 \times 1$ filters was used to apply the concatenated features. Then, two convolutional layers with 32 $3 \times 3$ filters were used to filter the multiscale features. After each convolutional layer, a $2 \times 2$ max-pooling layer was placed. Batch normalization was used to normalize the extracted features after the last convolutional layer. The normalized features were entered into the last block with two fully connected layers containing 64 and 280,280 neurons. With the exception of the last fully connected layer, which uses the sigmoid function, the other remaining layers use the ReLU activation function. The sigmoid function can define the dust-storm probability for each pixel.

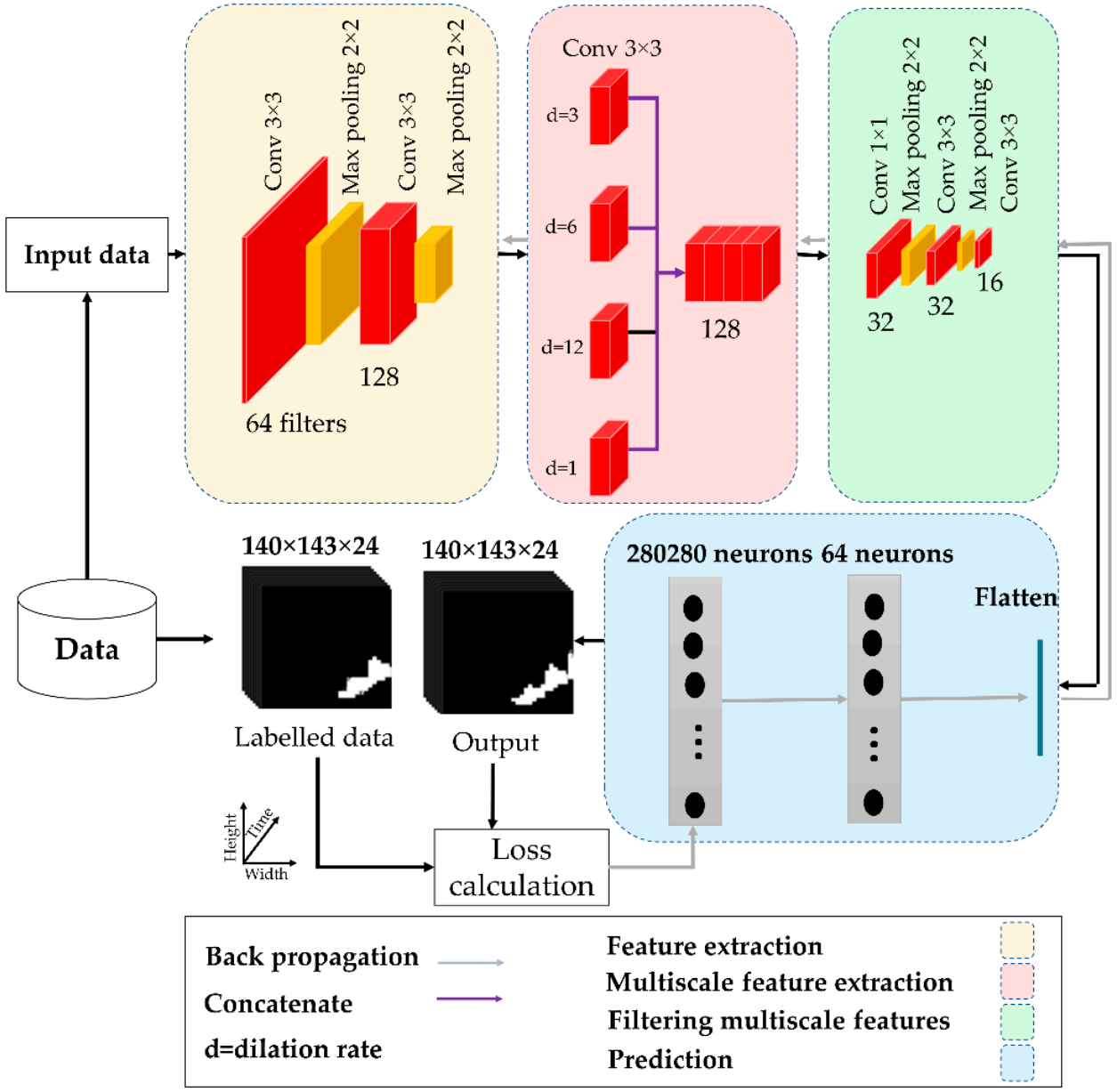


**Figure 4.** Proposed CNN architecture for prediction of transport pathway of dust storm.

### *2.4. Evaluation*

A dust-storm pathway prediction model can be evaluated using several metrics. Three measures, the overall accuracy, kappa coefficient, and F1 score, were used to evaluate the performance of the CNN model. These indices were obtained using a confusion matrix. The overall accuracy indicates the number of image regions that are correctly predicted. This index is obtained from Equation (2).

$$\text{Overall Accuracy}(\%) = \left(\frac{\text{TP} + \text{TN}}{\text{TP} + \text{FP} + \text{FN} + \text{TN}}\right) \times 100\% \quad (2)$$

where true positives (TP) are positive outcomes that are correctly predicted, and true negatives (TN) are negative outcomes that are correctly predicted by the model. False positives (FP) are positive results that the model has incorrectly predicted and are also known as type one errors, and false negatives (FN) are negative results that the model has incorrectly predicted (for more details, see [59]).

The Kappa coefficient shows the degree of agreement between the predicted data and reference data. A value of one for the Kappa coefficient indicates 100% agreement, and a value of zero indicates no agreement. The Kappa coefficient is obtained using Equation (3).

$$k = \frac{\rho_o - \rho_e}{1 - \rho_e} \tag{3}$$

where $\rho_o$ indicates the relative agreement between the two evaluators, and $\rho_e$ indicates the amount of expected agreement. These values are calculated using a confusion matrix (for more details, see [59,60]).

The F1 score is a useful quantitative measure of the balance between precision and recall. The F1 score is calculated using Equation (4) (for more details, see [61,62]):

$$F1(\%) = \left(2 \times \frac{\text{Precision} \times \text{Recall}}{\text{Precision} + \text{Recall}}\right) \times 100\% \tag{4}$$

Precision and recall are calculated using Equations (5) and (6), respectively.

$$\text{Precision}(\%) = \left(\frac{TP}{TP + FP}\right) \times 100\% \tag{5}$$

$$\text{Recall}(\%) = \left(\frac{TP}{TP + FN}\right) \times 100\% \tag{6}$$

## 3. Results

Machine-learning models have a wide range of hyperparameters. In order to train a CNN for accurate image classification, many hyperparameters must be adjusted, which can affect the network performance [63]. In this study, the hyperparameters have been tuned and a batch size of 16 was considered. A stochastic gradient descent (SGD) [64] optimizer with a learning rate of 0.0005 and 160 iterations were used during training. Dust-storm pathway prediction was trained using the Tversky loss function [65]. The test data, which were not involved in the training process, were used to prove the efficiency of the model. The loss function values for the training and validation data over 200 epochs are shown in Figure 5. The dynamics of a learning curve can be used to diagnose the behavior of a machine-learning model. As shown in Figure 5, the loss function exhibits a decreasing trend, indicating the positive performance of the model. The Tversky validation and training loss drastically decreased throughout the first epochs but gradually decreased between the 80th and 160th iterations. Normally, there is a gap between the training and validation loss learning curves. In an ideal fit, the plot of the validation loss decreases to a point of stability and exhibits a small gap with the training loss [66].

Relevant contextual information was selected using the RFFI. This information has a major impact on dust-storm occurrence and movement, which can contribute to improving prediction accuracy. Figure 6 shows the results of the RFFI. The 10-m and 50-m above-ground wind directions had the least influence on our prediction; therefore, they were excluded from the prediction process. Relative humidity, surface air temperature, surface wind direction, surface skin temperature, and surface wind speed had the most influence on the dust-storm pathway and were considered in the prediction (it should be noted that the U and V wind components were combined into single wind vectors in this analysis).

In order to examine the impact of geographic-context information on dust-storm prediction, the CNN model was trained with and without the context information (relative humidity, surface air temperature, surface wind direction, surface skin temperature, and surface wind speed). Confusion matrices were generated to evaluate the classification accuracy. Figure 7 shows a summary of the prediction results for t + 6, t + 12, t + 18, and t + 24 h when only spatial data (i.e., raw AOD data) were considered. The confusion matrix

shows that a high percentage of pixels are located along the diagonals. On average, more than 92% and 97% of pixels are correctly labeled as dust and non-dust, respectively. It should be noted that the prediction accuracy of the model is almost constant for every hour up to 24 h.

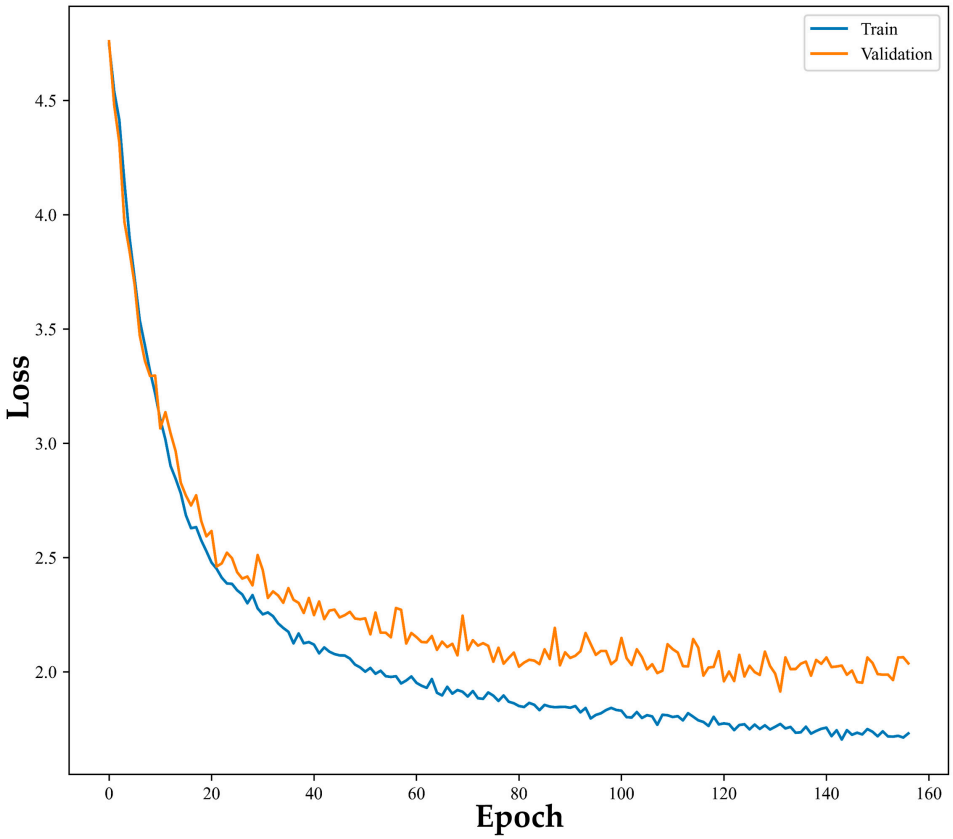


**Figure 5.** Training and validation loss over 200 epochs.

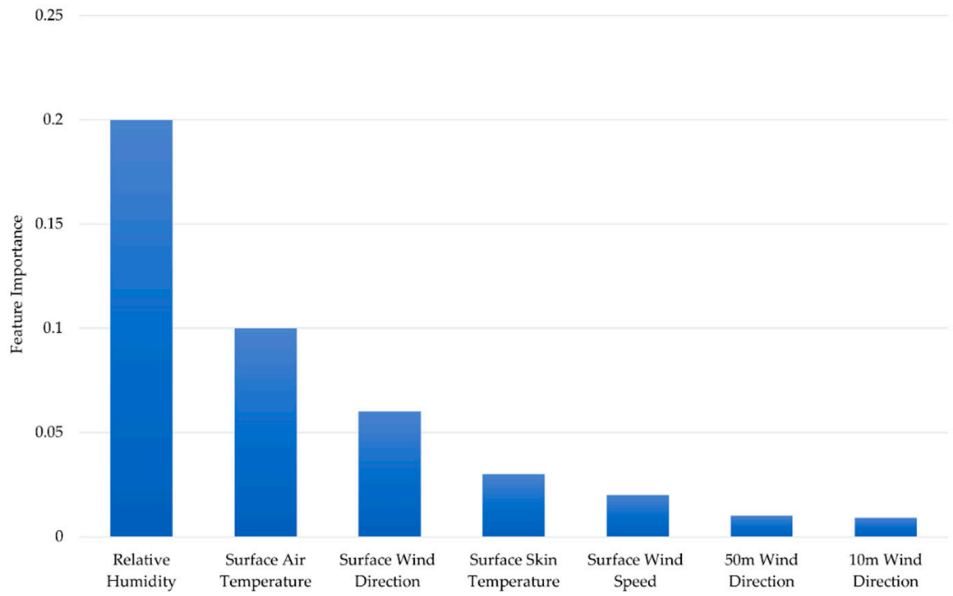


**Figure 6.** Feature importance values (based on MDI)).

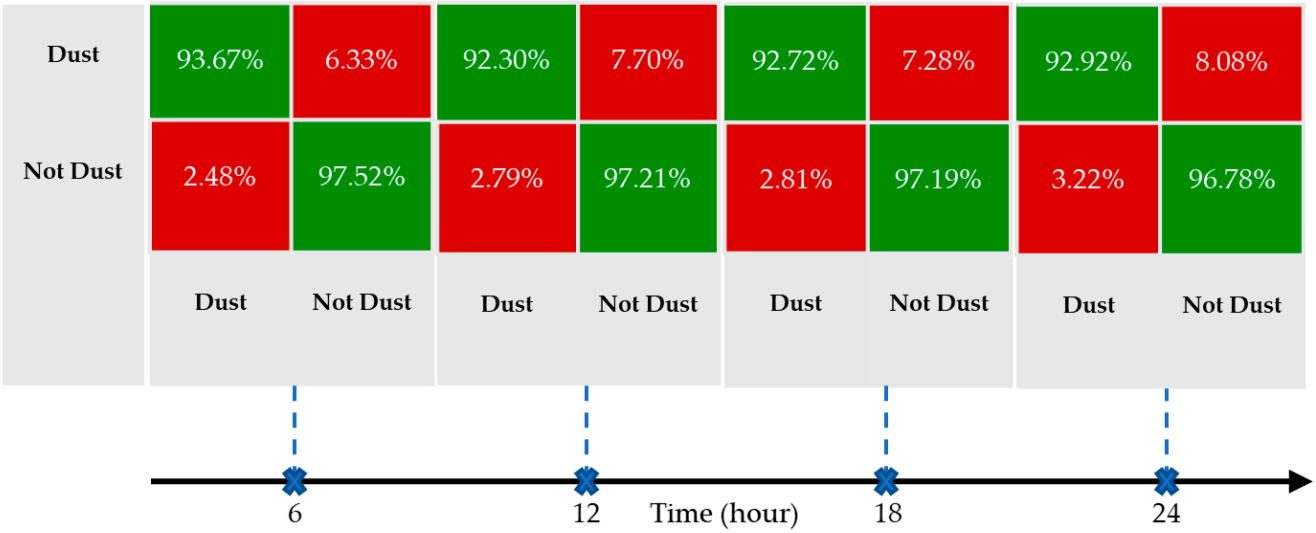


**Figure 7.** Confusion matrices based on only spatial data for 6, 12, 18, and 24 h.

Figure 8 shows the confusion matrices of the prediction model for t + 6, t + 12, t + 18, and t + 24 h after adding contextual information to the model. It can be observed that the number of pixels that are correctly labeled as dust increases; however, the number of pixels that are correctly labeled as not dust remains almost constant. This confirms the positive role of the geographic context in dust-storm pathway prediction.

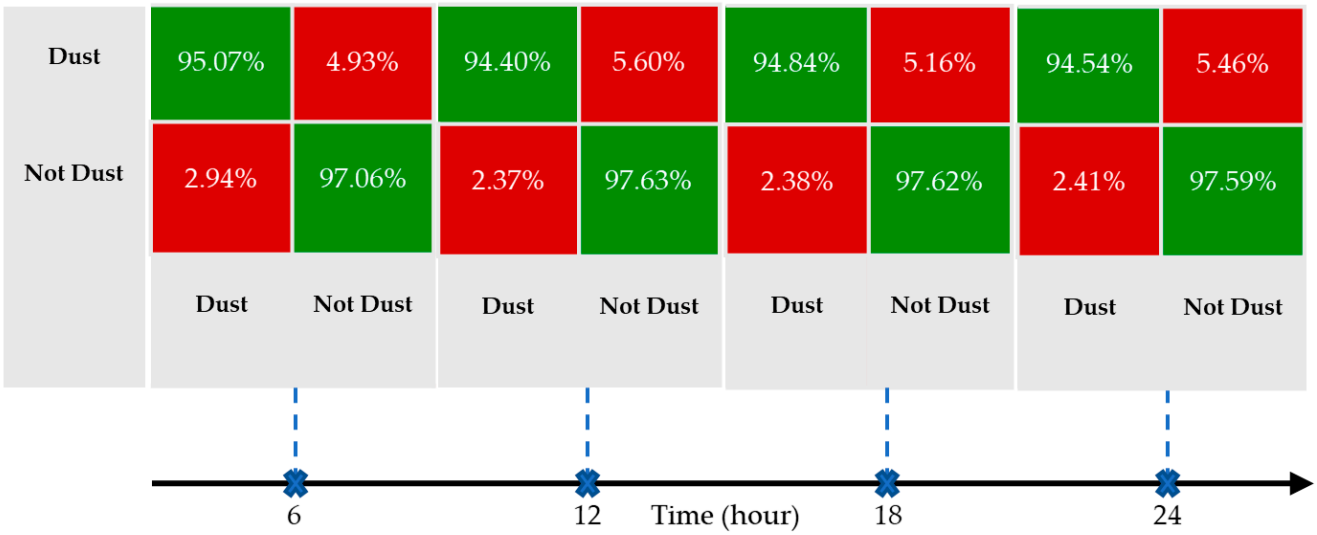


**Figure 8.** Confusion matrices based on spatial data and geographic-context information for 6, 12, 18, and 24 h.

The performance of the proposed CNN model for dust-storm transport pathway prediction is evaluated using the overall accuracy, kappa coefficient, and F1 score measures obtained from the confusion matrices. Figure 9 shows these metrics for t + 6, t + 12, t + 18, and t + 24 h when geographic information was considered. The overall accuracy, kappa coefficient, and F1 score had acceptable values for all anticipated hours. The performance of the CNN model was evaluated by the closeness of these values to 1. An overall accuracy of 0 indicates that the classifier always predicts incorrectly, whereas an accuracy of 1 indicates that it always predicts the correct label. For t + 6, t + 12, t + 18, and t + 24 h, the overall accuracies were 0.9746, 0.975, 0.9751, and 0.9699, respectively, which were close to 1. The highest possible value of the F1 score is 1, indicating perfect precision and recall, and the lowest possible value is 0 if either precision or recall is 0. An F1 score of 1 indicates

that the model correctly identifies all positive instances and does not produce any false positives or false negatives. The F1 scores of the model for the anticipated hours were 0.7497, 0.7525, 0.7476, and 0.6769, respectively, indicating the model's promising performance. A kappa coefficient of 1 indicates perfect agreement between the two measures. The kappa coefficients of the model for the anticipated hours were measured as 0.7369, 0.77, 0.7351, and 0.6625, respectively, which means there was a substantial level of agreement between the predicted and actual values and the results were reliable and consistent.

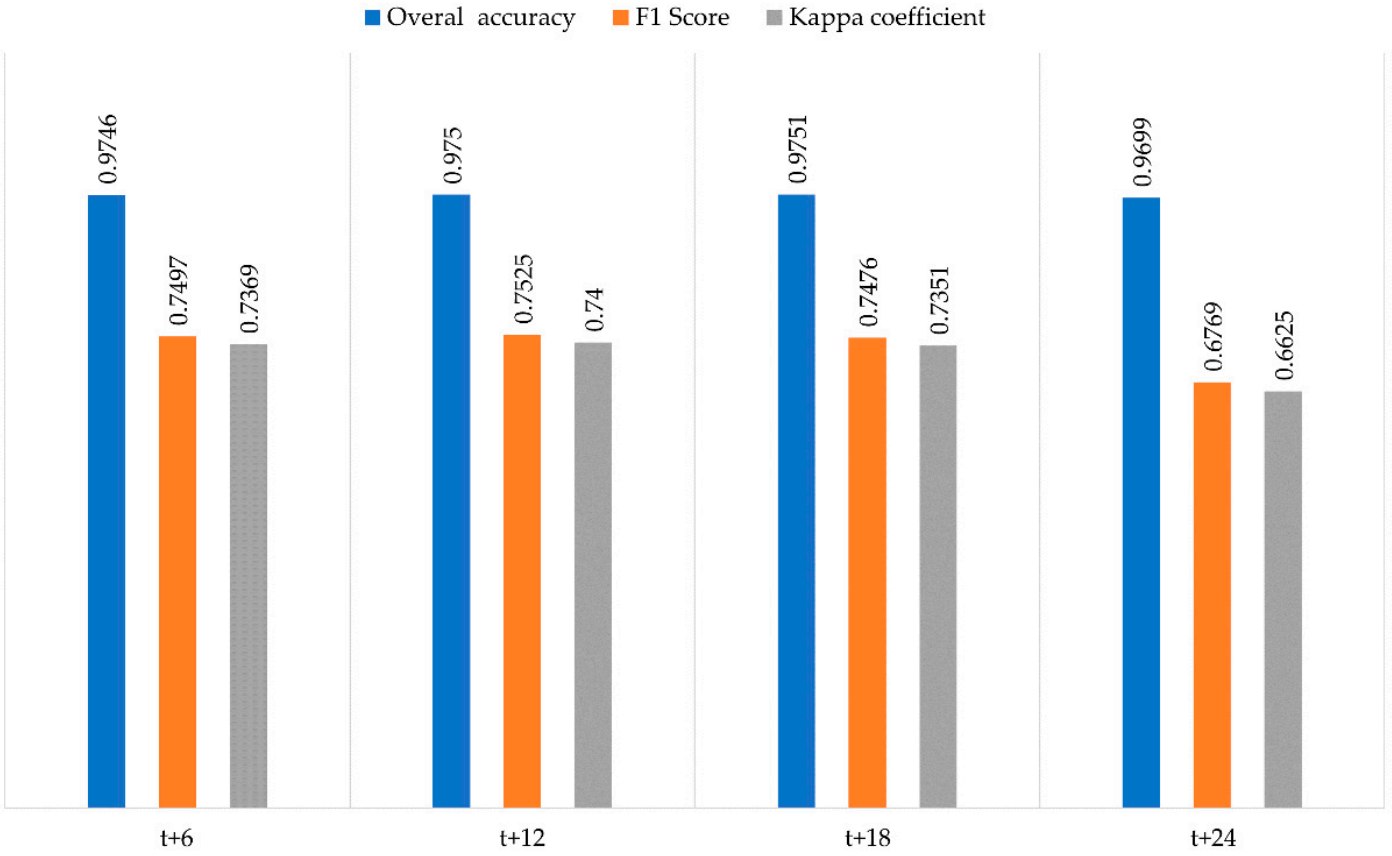


**Figure 9.** Evaluation indices for the next 6, 12, 18, and 24 h.

The predicted and actual shapes of a sample dust storm in Pakistan (that exists in our test dataset) at the 1st, 6th, 12th, 18th, and 24th hour are shown in Figure 10 as an example.

The predicted pathway of dust storms indicates which cities in the study area are more susceptible to dust storms' impact and require enhanced preparation and mitigation measures. Figure 11 shows the susceptibility of cities in the study area to dust storms (produced according to the prediction based on the dust storm records in our test dataset) originated in Pakistan and Turkmenistan. By executing the 24-h prediction for the dust storms in the test dataset and computing the frequency of storm hours that each city may experience, the susceptibility of cities to dust storms was calculated. In this case study, our focus was only on cities with a population exceeding 50,000 (i.e., major cities) situated along the predicted pathway of dust storms. The map illustrates these cities using red circles for those expected to be affected by dust storms originating in Pakistan and blue circles for those expected to be affected by dust storms originating in Turkmenistan. The size of each circle represents the frequency of storm hours that the respective city may experience.

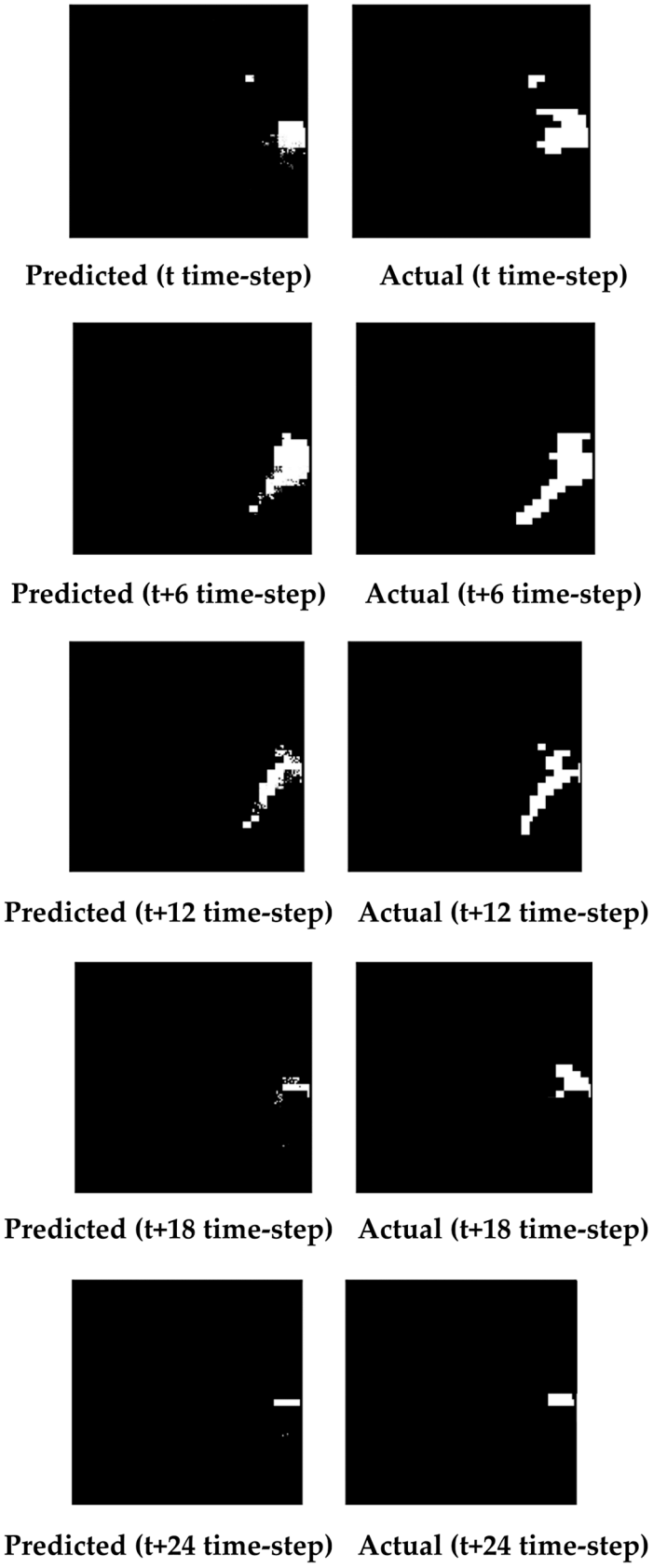


**Figure 10.** Predicted and actual results for a sample dust storm in Pakistan at the 1st, 6th, 12th, 18th, and 24th hour (dust storm pixels were shown in white and not dust storm pixels were shown in black).

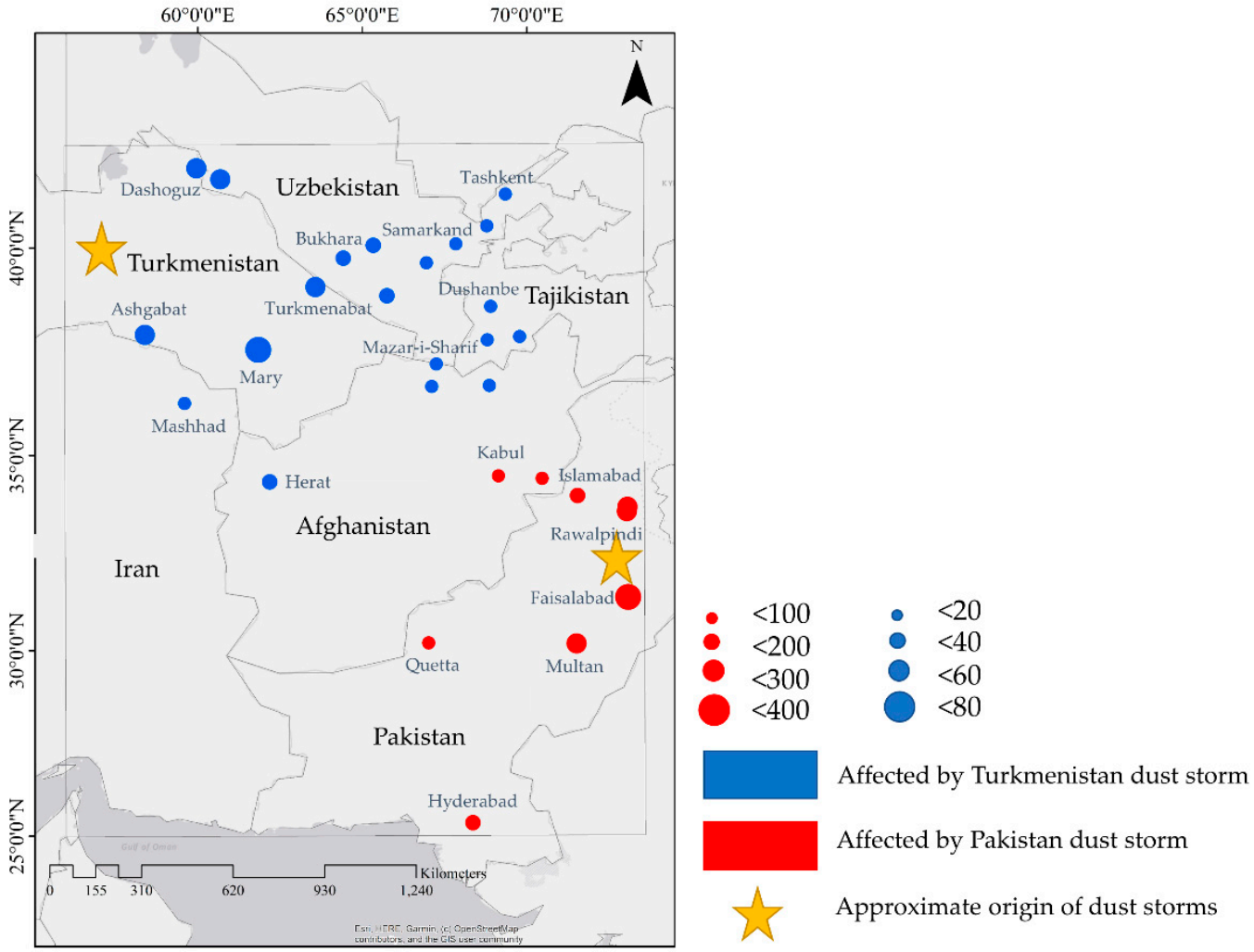


**Figure 11.** Dust storm susceptibility map for the major cities in the case study based on 24-h prediction (produced according to the prediction based on the test dataset).

## 4. Discussion

The proposed CNN model has several strengths, which make it a promising tool for predicting dust storms. One of its most significant advantages is the ability to predict dust storms on an hourly basis, as well as to extract a pathway with promising quality for the following 24 h. The computed performance metrics indicate that the model predictions are not only considerably accurate but also reliable, with a substantial level of agreement between the predicted and observed values. It should be noted that this level of accuracy was achieved despite the model using only one previous time step for prediction. However, the model's performance deteriorates when attempting to increase the prediction time because this exceeds the model's complexity and parameters. The contribution of the model in predicting dust storms can be attributed to its ability to extract multiscale features. This is particularly important given the wide range of storm sizes in the data, as the model can extract the relevant features for each size. Despite these strengths, the proposed model has several limitations. The CNN model used in this study required a large amount of computational power to train. In addition, because the CNN model lacks a memory cell, it cannot store historical data for an extended period, making it impossible to use the previous storm hours for more accurate predictions.

From the dataset perspective, the spatial resolution of $0.5^\circ \times 0.625^\circ$ of MERRA-2 may reduce the prediction accuracy. The MERRA-2 dataset is based on numerical weather prediction models, which may not fully capture all aspects of the real atmosphere. Despite

these limitations, it has a high temporal resolution of 1 h, allowing for hourly prediction of dust storms. Moreover, MERRA-2 provides data from 1980 to the present, which makes long-term analysis possible.

Previous studies on predicting the movement of dust storms have primarily utilized trajectory analysis approaches and the NOAA HYSPLIT model dataset. However, in this study, a CNN model based on the MERRA-2 dataset was employed. Previous results have indicated that the differences between the predicted and actual transport distances using the HYSPLIT model after 24 h fall within a range of 10% to 20% [67], and the accuracy of the model was primarily dependent on the quality of the meteorological data used. In contrast, our approach yielded better results and was less dependent on the meteorological data. However, the HYSPLIT model simplifies the emission characteristics of dust storms to increase computational efficiency. This model assumes a single point or small area as the origin of dust. By adopting this approach, the model can estimate the overall impact of dust storms on the atmosphere by treating the emissions originating from a single point, instead of modeling the entire dust storm as a complex and distributed source.

The effectiveness of the CNN method in predicting processes has been established in other applications, such as wildfire-spread and oil-spill modeling. In a similar study, a CNN model was used to predict the occurrence of a dust storm, achieving an overall accuracy of 0.883 [68]. These results support the effectiveness of the CNN model in predicting dust storms and suggest its potential use in other applications.

## 5. Conclusions

This study aimed to develop an accurate spatiotemporal model for dust-storm transport pathway prediction. In this regard, a hybrid CNN model that enabled the prediction of the hourly transport pathway of dust storms was developed. The model utilized raw MERRA-2 AOD data and various geographic-context information, including relative humidity, surface air temperature, surface wind direction, surface skin temperature, and surface wind speed, and labeled storm images as inputs. The CNN model extracted high-level features and contributed to the learning of dust-storm patterns. The results of the proposed CNN-based model showed a promising predictive power for prediction of the transport pathway of dust storms for up to 24 h in the selected study area. It was found that considering geographic information can improve the prediction accuracy. Compared with other available datasets, the MERRA-2 dataset has a high temporal resolution of one hour and global coverage, which enabled us to predict dust-storm pathways hourly. However, the CNN model did not have a memory cell, making it impossible to use the history of the storm to predict the subsequent hours. This limitation can be addressed using deep-learning methods with memory, such as LSTM, which can learn long-term dependencies between time steps and lead to more accurate results. The development of a hybrid CNN–LSTM model for dust-storm prediction is a promising topic for future research. This model can benefit from CNNs' feature-extraction abilities and LSTMs' long-term dependency learning characteristics.

**Author Contributions:** Conceptualization, M.S. and A.A.A.; methodology, M.Y. and M.S.; software, M.Y.; validation, M.Y.; formal analysis, M.Y. and M.S.; data curation, M.Y.; writing—original draft preparation, M.Y. and M.S.; writing—review and editing, M.S., A.A.A. and H.V.; supervision, A.A.A.; project administration, H.V. All authors have read and agreed to the published version of the manuscript.

**Funding:** This research received no external funding.

**Data Availability Statement:** The data presented in this study are available on request from the corresponding author.

**Conflicts of Interest:** The authors declare no conflict of interest.

## References


1. Harriman, L.M. Climate change implications and use of early warning systems for global dust storms. In *Reducing Disaster: Early Warning Systems For Climate Change*; Springer: Berlin/Heidelberg, Germany, 2014; pp. 153–165.
2. Sand and Dust Storms. Available online: https://public.wmo.int/en/our-mandate/focus-areas/environment/sand-and-dust-storms (accessed on 18 March 2023).
3. Rashki, A.; Kaskaoutis, D.G.; Francois, P.; Kosmopoulos, P.; Legrand, M. Dust-storm dynamics over Sistan region, Iran: Seasonality, transport characteristics and affected areas. *Aeolian Res.* **2015**, *16*, 35–48. [CrossRef]
4. Boloorani, A.D.; Shorabeh, S.N.; Samany, N.N.; Mousivand, A.; Kazemi, Y.; Jaafarzadeh, N.; Zahedi, A.; Rabiei, J. Vulnerability mapping and risk analysis of sand and dust storms in Ahvaz, IRAN. *Environ. Pollut.* **2021**, *279*, 116859. [CrossRef] [PubMed]
5. Shao, Y.; Wyrwoll, K.-H.; Chappell, A.; Huang, J.; Lin, Z.; McTainsh, G.H.; Mikami, M.; Tanaka, T.Y.; Wang, X.; Yoon, S.-C. Dust cycle: An emerging core theme in Earth system science. *Aeolian Res.* **2011**, *2*, 181–204. [CrossRef]
6. Darvishi Boloorani, A.; Soleimani, M.; Papi, R.; Neysani Samany, N.; Teymouri, P.; Soleimani, Z. Sources, Drivers, and Impacts of Sand and Dust Storms: A Global View. In *Dust and Health: Challenges and Solutions*; Springer: Berlin/Heidelberg, Germany, 2023; pp. 31–49.
7. Ai, N.; Polenske, K.R. Socioeconomic impact analysis of yellow-dust storms: An approach and case study for Beijing. *Econ. Syst. Res.* **2008**, *20*, 187–203. [CrossRef]
8. Tozer, P.; Leys, J. Dust storms–what do they really cost? *Rangel. J.* **2013**, *35*, 131–142. [CrossRef]
9. Baddock, M.; Strong, C.L.; Murray, P.S.; McTainsh, G.H. Aeolian dust as a transport hazard. *Atmos. Environ.* **2013**, *71*, 7–14. [CrossRef]
10. Darvishi Boloorani, A.; Soleimani, Z.; Teymouri, P.; Neysani Samany, N.; Soleimani, M.; Papi, R. Microbiology of Sand and Dust Storms and the Effects on Human Health in Iran and Other Persian Gulf Countries. In *Dust and Health: Challenges and Solutions*; Springer: Berlin/Heidelberg, Germany, 2023; pp. 157–186.
11. Lee, J.W.; Lee, K.K. Effects of Asian dust events on daily asthma patients in Seoul, Korea. *Meteorol. Appl.* **2014**, *21*, 202–209. [CrossRef]
12. Aghababaeian, H.; Ostadtaghizadeh, A.; Ardalan, A.; Asgary, A.; Akbary, M.; Yekaninejad, M.S.; Sharafkhani, R.; Stephens, C. Effect of dust storms on Non-Accidental, cardiovascular, and respiratory mortality: A Case of Dezful City in Iran. *Environ. Health Insights* **2021**, *15*, 11786302211060152. [CrossRef]
13. Ahmadzai, H.; Malhotra, A.; Tutundjian, S. Assessing the impact of sand and dust storm on agriculture: Empirical evidence from Mongolia. *PLoS ONE* **2023**, *18*, e0269271. [CrossRef]
14. Middleton, N. Dust storm hazards. In Proceedings of the Central Asian DUst Conference (CADUC 2019), Dushanbe, Tajikistan, 8–12 April 2019; p. 04001. Available online: https://www.e3s-conferences.org/articles/e3sconf/abs/2019/25/e3sconf_caduc2019_04001/e3sconf_caduc2019_04001.html (accessed on 18 March 2023).
15. Wei, X.; Chang, N.-B.; Bai, K.; Gao, W. Satellite remote sensing of aerosol optical depth: Advances, challenges, and perspectives. *Crit. Rev. Environ. Sci. Technol.* **2020**, *50*, 1640–1725. [CrossRef]
16. Mohammadpour, K.; Rashki, A.; Sciortino, M.; Kaskaoutis, D.G.; Boloorani, A.D. A statistical approach for identification of dust-AOD hotspots climatology and clustering of dust regimes over Southwest Asia and the Arabian Sea. *Atmos. Pollut. Res.* **2022**, *13*, 101395. [CrossRef]
17. Zhang, X.-X.; Sharratt, B.; Liu, L.-Y.; Wang, Z.-F.; Pan, X.-L.; Lei, J.-Q.; Wu, S.-X.; Huang, S.-Y.; Guo, Y.-H.; Li, J. East Asian dust storm in May 2017: Observations, modelling, and its influence on the Asia-Pacific region. *Atmos. Chem. Phys.* **2018**, *18*, 8353–8371. [CrossRef]
18. Kaskaoutis, D.; Prasad, A.K.; Kosmopoulos, P.; Sinha, P.; Kharol, S.; Gupta, P.; El-Askary, H.; Kafatos, M. Synergistic use of remote sensing and modeling for tracing dust storms in the Mediterranean. *Adv. Meteorol.* **2012**, *2012*, 861026. [CrossRef]
19. Li, L.; Liu, Y.; Wang, Y. Monitoring an air pollution episode in Shenzhen by combining MODIS satellite images and the HYSPLIT model. *IOP Conf. Ser. Earth Environ. Sci.* **2017**, *74*, 012010. [CrossRef]
20. Global Modeling and Assimilation Office. Available online: https://gmao.gsfc.nasa.gov/reanalysis/MERRA-2/ (accessed on 18 March 2023).
21. Wang, T.; Tang, J.; Sun, M.; Liu, X.; Huang, Y.; Huang, J.; Han, Y.; Cheng, Y.; Huang, Z.; Li, J. Identifying a transport mechanism of dust aerosols over South Asia to the Tibetan Plateau: A case study. *Sci. Total Environ.* **2021**, *758*, 143714. [CrossRef] [PubMed]
22. Sharif, M.; Alesheikh, A.A.; Tashayo, B. CaFIRST: A context-aware hybrid fuzzy inference system for the similarity measure of multivariate trajectories. *J. Intell. Fuzzy Syst.* **2019**, *36*, 5383–5395. [CrossRef]
23. Boroumand, F.; Alesheikh, A.A.; Sharif, M.; Farnaghi, M. FLCSS: A fuzzy-based longest common subsequence method for uncertainty management in trajectory similarity measures. *Trans. GIS* **2022**, *26*, 2244–2262. [CrossRef]
24. Goudarzi, S.; Sharif, M.; Karimipour, F. A context-aware dimension reduction framework for trajectory and health signal analyses. *J. Ambient. Intell. Humaniz. Comput.* **2022**, *13*, 2621–2635. [CrossRef]
25. NOAA Air Resources Laboratory. Available online: https://www.ready.noaa.gov/HYSPLIT.php (accessed on 18 March 2023).
26. McGowan, H.; Clark, A. Identification of dust transport pathways from Lake Eyre, Australia using Hysplit. *Atmos. Environ.* **2008**, *42*, 6915–6925. [CrossRef]
27. Aili, A.; Xu, H.; Kasim, T.; Abulikemu, A. Origin and transport pathway of dust storm and its contribution to particulate air pollution in northeast edge of Taklimakan Desert, China. *Atmosphere* **2021**, *12*, 113. [CrossRef]

28. Guan, Q.; Yang, Y.; Luo, H.; Zhao, R.; Pan, N.; Lin, J.; Yang, L. Transport pathways of PM10 during the spring in northwest China and its characteristics of potential dust sources. *J. Clean. Prod.* **2019**, *237*, 117746. [CrossRef]
29. Aili, A.; Abuduwaili, J.; Xu, H.; Zhao, X.; Liu, X. A Cluster Analysis of Forward Trajectory to Identify the Transport Pathway of Salt-Dust Particles from Dried Bottom of Aral Sea, Central Asia. *Atmosphere* **2021**, *12*, 764. [CrossRef]
30. Stein, A.; Draxler, R.R.; Rolph, G.D.; Stunder, B.J.; Cohen, M.; Ngan, F. NOAA's HYSPLIT atmospheric transport and dispersion modeling system. *Bull. Am. Meteorol. Soc.* **2015**, *96*, 2059–2077. [CrossRef]
31. Sharif, M.; Alesheikh, A.A. Context-aware movement analytics: Implications, taxonomy, and design framework. *Wiley Interdiscip. Rev. Data Min. Knowl. Discov.* **2018**, *8*, e1233. [CrossRef]
32. Dodge, S. Context-dependent movement analysis. In *Handbook of Spatial Analysis in the Social Sciences*; Edward Elgar Publishing: Cheltenham, UK, 2022; pp. 187–207.
33. Miri, A.; Maleki, S.; Middleton, N. An investigation into climatic and terrestrial drivers of dust storms in the Sistan region of Iran in the early twenty-first century. *Sci. Total Environ.* **2021**, *757*, 143952. [CrossRef]
34. Perumal, R.; van Zyl, T.L. Comparison of recurrent neural network architectures for wildfire spread modelling. In Proceedings of the 2020 International SAUPEC/RobMech/PRASA Conference, Cape Town, South Africa, 29–31 January 2020; pp. 1–6.
35. Marjani, M.; Mesgari, M. The Large-Scale Wildfire Spread Prediction Using a Multi-Kernel Convolutional Neural Network. *ISPRS Ann. Photogramm. Remote Sens. Spat. Inf. Sci.* **2023**, *14*, 483–488. [CrossRef]
36. Burge, J.; Bonanni, M.; Ihme, M.; Hu, L. Convolutional LSTM neural networks for modeling wildland fire dynamics. *arXiv* **2020**, arXiv:2012.06679.
37. Wang, R.; Zhu, Z.; Zhu, W.-H.; Fu, X.; Xing, S. A Dynamic Marine Oil Spill Prediction Model Based on Deep Learning. *J. Coast. Res.* **2021**, *37*, 716–725. [CrossRef]
38. Jiao, Z.; Jia, G.; Cai, Y. A new approach to oil spill detection that combines deep learning with unmanned aerial vehicles. *Comput. Ind. Eng.* **2019**, *135*, 1300–1311. [CrossRef]
39. NASA Earth Observatory. *A Dusty Spring Day in Turkmenistan*; NASA: Washington, DC, USA, 2022.
40. Orlovsky, L.; Orlovsky, N.; Durdyev, A. Dust storms in Turkmenistan. *J. Arid. Environ.* **2005**, *60*, 83–97. [CrossRef]
41. Rienecker, M.M.; Suarez, M.J.; Gelaro, R.; Todling, R.; Bacmeister, J.; Liu, E.; Bosilovich, M.G.; Schubert, S.D.; Takacs, L.; Kim, G.-K. MERRA: NASA's modern-era retrospective analysis for research and applications. *J. Clim.* **2011**, *24*, 3624–3648. [CrossRef]
42. Yousefi, R.; Wang, F.; Ge, Q.; Shaheen, A. Long-term aerosol optical depth trend over Iran and identification of dominant aerosol types. *Sci. Total Environ.* **2020**, *722*, 137906. [CrossRef] [PubMed]
43. Qin, W.; Liu, Y.; Wang, L.; Lin, A.; Xia, X.; Che, H.; Bilal, M.; Zhang, M. Characteristic and driving factors of aerosol optical depth over mainland China during 1980–2017. *Remote Sens.* **2018**, *10*, 1064. [CrossRef]
44. Sun, E.; Xu, X.; Che, H.; Tang, Z.; Gui, K.; An, L.; Lu, C.; Shi, G. Variation in MERRA-2 aerosol optical depth and absorption aerosol optical depth over China from 1980 to 2017. *J. Atmos. Sol.-Terr. Phys.* **2019**, *186*, 8–19. [CrossRef]
45. Fu, Y.; Huang, T.S. Unsupervised locally embedded clustering for automatic high-dimensional data labeling. In Proceedings of the 2007 IEEE International Conference on Acoustics, Speech and Signal Processing-ICASSP'07, Honolulu, HI, USA, 15–20 April 2007; pp. III-1057–III-1060.
46. Otsu, N. A threshold selection method from gray-level histograms. *IEEE Trans. Syst. Man Cybern.* **1979**, *9*, 62–66. [CrossRef]
47. Breiman, L. Random Forests. *Mach. Learn.* **2001**, *45*, 5–32. [CrossRef]
48. Louppe, G.; Wehenkel, L.; Sutera, A.; Geurts, P. Understanding variable importances in forests of randomized trees. *Adv. Neural Inf. Process. Syst.* **2013**, *1*, 431–439.
49. Scornet, E. Trees, forests, and impurity-based variable importance. *arXiv* **2020**, arXiv:2001.04295. [CrossRef]
50. Patro, S.; Sahu, K.K. Normalization: A preprocessing stage. *arXiv* **2015**, arXiv:1503.06462. [CrossRef]
51. LeCun, Y.; Boser, B.E.; Denker, J.S.; Henderson, D.; Howard, R.E.; Hubbard, W.E.; Jackel, L.D. Backpropagation Applied to Handwritten Zip Code Recognition. *Neural Comput.* **1989**, *1*, 541–551. [CrossRef]
52. Krizhevsky, A.; Sutskever, I.; Hinton, G.E. ImageNet classification with deep convolutional neural networks. *Commun. ACM* **2012**, *60*, 84–90. [CrossRef]
53. Du, S.; Li, T.; Yang, Y.; Horng, S.-J. Deep air quality forecasting using hybrid deep learning framework. *IEEE Trans. Knowl. Data Eng.* **2019**, *33*, 2412–2424. [CrossRef]
54. Alzubaidi, L.; Zhang, J.; Humaidi, A.J.; Al-dujaili, A.; Duan, Y.; Al-Shamma, O.; Santamaría, J.; Fadhel, M.A.; Al-Amidie, M.; Farhan, L. Review of deep learning: Concepts, CNN architectures, challenges, applications, future directions. *J. Big Data* **2021**, *8*, 53. [CrossRef] [PubMed]
55. Mahdianpari, M.; Salehi, B.; Rezaee, M.; Mohammadimanesh, F.; Zhang, Y. Very Deep Convolutional Neural Networks for Complex Land Cover Mapping Using Multispectral Remote Sensing Imagery. *Remote Sens.* **2018**, *10*, 1119. [CrossRef]
56. Kattenborn, T.; Leitloff, J.; Schiefer, F.; Hinz, S. Review on Convolutional Neural Networks (CNN) in vegetation remote sensing. *ISPRS J. Photogramm. Remote Sens.* **2021**, *173*, 24–49. [CrossRef]
57. Chollet, F. *Deep Learning with Python*; Simon and Schuster: New York, NY, USA, 2017.
58. Nair, V.; Hinton, G.E. Rectified linear units improve restricted boltzmann machines. In Proceedings of the 27th International Conference on Machine Learning (ICML-10), Haifa, Israel, 21–24 June 2010; pp. 807–814.

59. Fielding, A.H.; Bell, J.F. A review of methods for the assessment of prediction errors in conservation presence/absence models. *Environ. Conserv.* **1997**, *24*, 38–49. [CrossRef]
60. Vahidi, H.; Klinkenberg, B.; Yan, W. Trust as a proxy indicator for intrinsic quality of Volunteered Geographic Information in biodiversity monitoring programs. *GIScience Remote Sens.* **2018**, *55*, 502–538. [CrossRef]
61. Maxwell, A.E.; Warner, T.A.; Guillén, L.A. Accuracy assessment in convolutional neural network-based deep learning remote sensing studies—Part 1: Literature review. *Remote Sens.* **2021**, *13*, 2450. [CrossRef]
62. Vahidi, H.; Klinkenberg, B.; Johnson, B.A.; Moskal, L.M.; Yan, W. Mapping the individual trees in urban orchards by incorporating volunteered geographic information and very high resolution optical remotely sensed data: A template matching-based approach. *Remote Sens.* **2018**, *10*, 1134. [CrossRef]
63. Kandel, I.; Castelli, M. The effect of batch size on the generalizability of the convolutional neural networks on a histopathology dataset. *ICT Express* **2020**, *6*, 312–315. [CrossRef]
64. Bottou, L. Stochastic gradient descent tricks. In *Neural Networks: Tricks of the Trade*, 2nd ed.; Springer: Berlin/Heidelberg, Germany, 2012; pp. 421–436.
65. Salehi, S.S.M.; Erdogmus, D.; Gholipour, A. Tversky loss function for image segmentation using 3D fully convolutional deep networks. In Proceedings of the Machine Learning in Medical Imaging: 8th International Workshop, MLMI 2017, Held in Conjunction with MICCAI 2017, Quebec City, QC, Canada, 10 September 2017; pp. 379–387.
66. Smith, L.N. A disciplined approach to neural network hyper-parameters: Part 1–learning rate, batch size, momentum, and weight decay. *arXiv* **2018**, arXiv:1803.09820.
67. Draxler, R.R.; Hess, G. An overview of the HYSPLIT_4 modelling system for trajectories. *Aust. Meteorol. Mag.* **1998**, *47*, 295–308.
68. Tiancheng, L.; Qing-dao-er-ji, R.; Ying, Q. Application of Improved Naive Bayesian-CNN Classification Algorithm in Sandstorm Prediction in Inner Mongolia. *Adv. Meteorol.* **2019**, *2019*, 5176576. [CrossRef]